

# INFLUENCE OF COLLISION ENERGY ON THE DYNAMICS OF THE REACTION $O(^1D) + CH_4(X^1A_1) \rightarrow OH(X^2\Pi) + CH_3(X^2A_2)$

R. Sayós<sup>(a)</sup> \*, Jordi Hernando<sup>(a)</sup>, María P. Puyuelo<sup>(b)</sup>, Pedro A. Enríquez<sup>(b)</sup>, and Miguel González<sup>(a)</sup> \*

<sup>(a)</sup> Departament de Química Física i Centre de Recerca en Química Teòrica, Universitat de Barcelona, C/ Martí i Franquès, 1. E-08028 Barcelona (Spain)

<sup>(b)</sup> Departamento de Química, Universidad de La Rioja, C/ Madre de Dios, 51. E-26004 Logroño (Spain)

## ABSTRACT

We studied the effects of collision energy ( $E_T$ ) on the dynamics of the title reaction using the quasiclassical trajectory method on an analytical triatomic potential energy surface we had derived for this system. We compared the dependence of the scalar and two-vector properties of the reaction on  $E_T$  with experimental data and obtained a quite good agreement. The results can be explained in terms of the coexistence of two microscopic reaction mechanisms: insertion and abstraction. The former mechanism is the most important one, although the contribution of the latter increases with  $E_T$ .

**Keywords:**  $O(^1D) + CH_4 \rightarrow OH + CH_3$  reaction, quasiclassical trajectories, influence of collision energy, dynamics

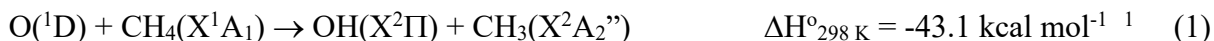
**Tables:** 2 **Figures:** 5

**Proofs to:** Prof. Miguel González

\*Authors for correspondence: r.sayos@qf.ub.es, miguel@qf.ub.es

## 1. INTRODUCTION

The reaction of methane with the oxygen atom in the first excited electronic state,



is an important source of stratospheric OH, which affects the chemistry of the earth's ozone layer through the HO<sub>x</sub> cycles<sup>2,3,4</sup>. The OH+CH<sub>3</sub> reaction channel is the most important one for the O(<sup>1</sup>D) + CH<sub>4</sub> reaction (the quantum yield is equal to 0.75 ± 0.15 at 300 K<sup>5</sup>), whose overall rate constant at room temperature approaches the gas kinetic limit:  $k = 1.5 \times 10^{-10} \text{ cm}^3 \text{ molecule}^{-1} \text{ s}^{-1}$ <sup>5</sup>.

The dynamics of reaction (1) has been studied experimentally. Laser-induced fluorescence (LIF) and chemiluminescence measurements of the internal state distributions of nascent OH have been carried out through the generation of the O(<sup>1</sup>D) atoms by photodissociation of either O<sub>3</sub> at 248/266 nm<sup>6,7,8,9,10</sup> (the mean collision energy of the system ( $\langle E_T \rangle$ ) being around 0.2 eV) or N<sub>2</sub>O at 193 nm<sup>11,12,13</sup> ( $\langle E_T \rangle = 0.40$  eV). Polarized Doppler-resolved LIF spectroscopy<sup>14,15,16,17,18</sup> was used to study the OH product state-resolved kinetic energy and angular distributions at  $\langle E_T \rangle = 0.40$  eV and, very recently, global product kinetic energy and angular distributions have been determined at  $E_T = 0.28$  eV using molecular beams<sup>19</sup>. The energy distribution of the CH<sub>3</sub> molecules produced in reaction (1) was also measured<sup>20,21</sup>.

Reaction (1) has also been studied theoretically. *Ab initio* calculations at several levels were reported for the lowest potential energy surface (1<sup>1</sup>A PES) of the O(<sup>1</sup>D) + CH<sub>4</sub> system<sup>22,23</sup>. Using *ab initio* data and treating the CH<sub>3</sub> group as a pseudoatom, we fitted two versions of a triatomic analytical surface to represent the 1<sup>1</sup>A PES (PES1<sup>23</sup> and PES2<sup>24</sup>). In addition, quasiclassical trajectory (QCT) calculations were performed on these PESs to examine internal state distributions of nascent OH and the stereodynamics in the reaction conditions explored experimentally ( $\langle E_T \rangle = 0.21$  and 0.40 eV)<sup>13,23-24</sup>.

In this work we performed a thorough dynamic study of reaction (1) using the QCT method and the analytical triatomic surface PES2 previously derived by us for the O(<sup>1</sup>D) + CH<sub>4</sub> system<sup>24</sup>. We examined the dependence on the collision energy of the scalar and two-vector properties of reaction (1). This allowed us to carry out a detailed analysis of the dynamic behavior for reaction conditions not attained in the experiments, and also to explore dynamical properties other than those studied in the experimental conditions, and to compare with the most recent experimental results reported about the O(<sup>1</sup>D) + CH<sub>4</sub> reaction<sup>19</sup>. Finally, the change of the dynamical behavior on varying  $E_T$  has been analyzed in terms of the microscopic reaction mechanism.

## 2. COMPUTATIONAL METHOD

The QCT method<sup>25,26,27</sup> was applied as implemented in the TRIQCT program<sup>28</sup> to study reaction (1), using the analytical triatomic potential energy surface PES2<sup>24</sup>. This analytical surface was fitted using *ab initio* data about the 1<sup>1</sup>A PES through which reaction (1) evolves, ensuring that the assumption of taking the CH<sub>3</sub> group as a pseudoatom of 15 a.m.u. (located in its center of mass) did not entail the appearance of a spurious reaction barrier<sup>24</sup>. This PES connects the O(<sup>1</sup>D) + CH<sub>4</sub> reactants with the OH + CH<sub>3</sub> products along a minimum energy path (MEP) that does not present an energy barrier above reactants. Also, it allows for either an abstraction microscopic mechanism or an insertion/elimination microscopic mechanism that evolves through the CH<sub>3</sub>OH minimum<sup>24</sup>.

In a previous study<sup>24</sup>, PES2 quite satisfactorily reproduced the dynamic behavior experimentally established for reaction (1) (final energy of the OH product and other properties such as rate constants, branching ratios, and also translational energy distributions and  $\mathbf{kk}'$  differential cross-sections for OH state-specific products). This was possible because PES2 efficiently describes the insertion/fast elimination mechanism, which is believed to be the most important one for this reaction<sup>9,12-13,19</sup>. Hence, the dynamic properties of the OH product arising from reaction (1) may be reproduced quite satisfactorily with the triatomic model considered. This kind of model has also been quite successfully applied in our group to the study of the O(<sup>1</sup>D) + N(NO)<sup>29</sup>, O(<sup>3</sup>P) + H(CH<sub>3</sub>)<sup>30,31</sup> and O(<sup>1</sup>D) + H(OH)<sup>32</sup> reactions.

The accuracy of the numerical integration of Hamilton's differential equations was verified by checking the conservation of total energy and total angular momentum in every trajectory, and performing back-integrations on some batches of trajectories. An integration step of  $2.5 \times 10^{-17}$  s and an initial distance of 10 Å between the O(<sup>1</sup>D) and the H-(CH<sub>3</sub>) centre of mass were selected. This separation ensures that the interaction energy is negligible compared to the available energy of reactants. The rovibrational levels of the OH product were assigned using the vibrational action variable method. As the QCT method does not account for the OH(X<sup>2</sup>Π) orbital ( $\Lambda=1$ ) and spin ( $S=1/2$ ) electronic angular momenta, we identified the total angular momentum quantum number excluding electronic and nuclear spins,  $N'$ , of the OH molecule with the value of the rotational angular momentum derived from the QCT calculations,  $j'$ , plus one.

Several collision energies were considered in the QCT study of reaction (1),  $E_T= 0.28, 0.60, 0.80, 1.0$  and  $1.4$  eV, thus completing our analysis at  $E_T= 0.21$  and  $0.40$  eV<sup>24</sup>. The results obtained at the new values of  $E_T$  in this study and those from the previous study<sup>24</sup> will be shown together. Around 200 000-300 000 trajectories were run for each new condition, so the statistical

errors estimated for all the calculated dynamic properties were very small. For each collision energy the rovibrational energy levels of the H-(CH<sub>3</sub>) pseudodiatom molecule were sampled according to a 298 K Maxwell-Boltzmann distribution, and the masses of the most abundant isotopes of the O, H and C atoms (<sup>16</sup>O, <sup>1</sup>H and <sup>12</sup>C) were considered in the calculations. However, for comparison with the experimental results reported in ref. 19, additional calculations were carried out using the <sup>18</sup>O isotope at the  $E_T = 0.28$  eV condition. Up to 1 000 000 trajectories were run in this case. Very small differences were found when either the <sup>16</sup>O mass or the <sup>18</sup>O mass was employed.

### 3. REACTION DYNAMICS

#### 3.1. Scalar properties

The scalar properties determined for reaction (1) are shown in figure 1. Figure 1a depicts the reaction cross-section,  $\sigma_r$ , as a function of  $E_T$  for both the global O(<sup>1</sup>D) + CH<sub>4</sub> reaction and the OH formation channel. To calculate  $\sigma_r$ , the values of the cross-sections derived from PES2 ( $\sigma_r^{\text{PES2}}$ ) were multiplied by 4 (to take into account that there are four equivalent hydrogen atoms in the methane molecule, which are assumed to react independently), and then divided by 5 (to account for the electronic degeneracy of the O(<sup>1</sup>D) + CH<sub>4</sub> asymptote). The values of  $\sigma_r$  for both the global reaction and the OH formation channel diminish with  $E_T$  increase (figure 1a), as expected for reactions without a barrier above reactants<sup>33</sup>. Up to  $E_T = 0.80$  eV the decrease in  $\sigma_r$  is due only to a reduction of the maximum reactive impact parameter ( $b_{\text{max}} = 4.2$  and  $3.5$  Å at 0.21 and 0.80 eV, respectively), since the reaction probability ( $P_r$ ) increases slightly with collision energy in this interval. For higher values of  $E_T$ ,  $b_{\text{max}}$  remains nearly constant and  $P_r$  diminishes. The contribution of the OH channel to the global reaction decreases slightly with  $E_T$  increase. Thus, the branching ratio of this product channel decreases from 0.64 at  $E_T = 0.21$  eV to 0.59 at  $E_T = 1.4$  eV. The triatomic model employed to study the O(<sup>1</sup>D) + CH<sub>4</sub> system cannot account for all possible reaction channels (only the OH + CH<sub>3</sub> and CH<sub>3</sub>O + H products are described). However, the global branching ratio measured for these two reaction channels is around 0.95<sup>19</sup>.

---

Figure 1. Scalar properties: excitation and opacity functions, average fractions of energy, and vibrational and rotational distributions.

---

The dependence of the reaction probability on the impact parameter ( $b$ ) (opacity function) was studied for the seven values of the collision energy considered. In figure 1b the opacity function is depicted for  $E_T= 0.28, 0.80$  and  $1.4$  eV, which roughly correspond to low, intermediate and high collision energy values. The opacity function for reaction (1) has a non-negligible dependence on  $E_T$ . For low collision energies, the reaction probability is almost constant up to values of  $b$  of around  $2.5 \text{ \AA}$ , after which it decreases monotonically. At higher collision energies, the reaction probability is much smaller for low impact parameters, its value increasing monotonically and reaching its maximum at larger values of the  $b/b_{max}$  ratio with higher  $E_T$ .

The OH vibrational distribution is depicted in figure 1d for  $E_T= 0.28, 0.80$  and  $1.4$  eV, and collected in table 1 for all the  $E_T$  values considered. These distributions are more excited than the statistically expected (prior distributions) and depend significantly on  $E_T$ . Thus, the monotonically decreasing vibrational distributions found for low and intermediate values of  $E_T$  transform into inverted distributions at the highest collision energies explored. The fraction of available energy channeled as OH vibration, however, remains nearly constant with  $E_T$  variation (figure 1c). For instance,  $\langle f_{v'} \rangle = 0.43$  and  $0.47$  for  $E_T= 0.21$  and  $1.4$  eV, respectively.

---

Table 1. Vibrational populations and average rotational levels.

---

The average fraction of available energy released as OH rotation does not change significantly with  $E_T$  variation (figure 1c), as it occurs in the case of the OH vibration. The average values are  $\langle f_{R'} \rangle = 0.23$  and  $0.21$  for  $E_T= 0.21$  and  $1.4$  eV, respectively. The average rotational levels for each populated vibrational level are given in table 1 for all  $E_T$  values considered, while figures 1e-1f depict the rotational distributions for low- $v'$  ( $v'=0$ ) and high- $v'$  ( $v'=5$ ) levels at  $E_T= 0.28, 0.80$  and  $1.4$  eV. For the lowest populated vibrational levels ( $v'=0-4$ ) the distributions are more excited than the statistical ones (prior distributions) and their population maxima appear at high- $N'$  values. The values of the most populated rotational level and of the highest rotational level reached diminish with the vibrational quantum number, as expected. On the other hand, though the OH( $v'=0-4$ ) rotational distributions are slightly more excited as  $E_T$  rises, they do not vary appreciably with collision energy. This can be attributed to the large exothermicity of the reaction and the depth of the minimum through which the reactivity mainly takes place. The OH rotational distributions for the highest vibrational levels ( $v' \geq 5$ ) are less excited than the ones for  $v' \leq 4$ , and their population maxima appear at low- $N'$

values. Moreover, they show a somewhat more pronounced dependence on  $E_T$ , the distributions becoming clearly more excited and displaying a clear bimodal feature as  $E_T$  increases.

The average fraction of available energy channeled as products relative translation is also nearly constant with  $E_T$  (figure 1c). The average value of the products relative translational energy ( $\langle E_T' \rangle$ ), however, clearly increases as collision energy rises, as expected due to the increasing amount of available energy ( $\langle E_T' \rangle = 0.69$  and  $1.0$  eV for  $E_T = 0.21$  and  $1.4$  eV, respectively). Figure 2a depicts the experimental<sup>19</sup> and calculated kinetic energy distributions at  $E_T = 0.28$  eV for the  $^{18}\text{OH} + \text{CH}_3$  products. Although both distributions have similar shape and maximum position, the QCT one is wider than the experimentally reported, indicating that more translational excitation is expected from the calculations ( $\langle E_T' \rangle = 0.52$  and  $0.70$  eV for the experimental and QCT data, respectively). This can be explained in terms of the triatomic model used, which neglects the internal degrees of freedom of the methyl fragment. As a result, the available energy can not be released as internal energy of the  $\text{CH}_3$  co-product, resulting in a higher fraction of energy channeled as translation. Nevertheless, the QCT and experimental  $E_T'$  distributions are similar. This, along with the fact that the triatomic model gives a quite good description of the internal energy distributions of the OH product<sup>24</sup>, suggests that little available energy should be expected to be channeled as  $\text{CH}_3$  internal excitation, as reported experimentally<sup>20-21</sup>. However, this is not fully accomplished if detailed OH state-specific channels of reaction (1) are considered. Thus, it was measured that for the reaction channel leading to  $\text{OH}(v'=0, N'=5, 19)^{17-18}$ , an important amount of the available energy was released as products kinetic energy, which was not reproduced by the triatomic model<sup>24</sup>. Otherwise, it was proved in the experiments that the production of vibrationally excited OH molecules ( $\text{OH}(v'=4, N'=8)$  channel) was accompanied by a minor translational excitation of products<sup>17-18</sup>, the triatomic model leading in this case to a good agreement with experiment.

---

Figure 2. Products translational energy distributions,  $\mathbf{kk}'$  DCSs and velocity-angle scattering distribution at  $E_T = 0.28$  eV.

---

### 3.2. Two-vector properties

The analysis of the total angular momentum ( $\mathbf{J}$ ) transformation from reactants to products was examined at all the collision energies considered. In all cases  $\mathbf{J} \approx \mathbf{l} \rightarrow \mathbf{l}'$ , as expected for a heavy-light-heavy (H-L-H) reaction

The angular distributions arising from reaction (1) for the two-vector correlations between initial ( $\mathbf{k}$ ) and final ( $\mathbf{k}'$ ) relative velocity vectors ( $\mathbf{k}\mathbf{k}'$ ), between  $\mathbf{k}$  and the final rotational angular momentum  $\mathbf{j}'$  ( $\mathbf{k}\mathbf{j}'$ ), between  $\mathbf{k}'$  and  $\mathbf{j}'$  ( $\mathbf{k}'\mathbf{j}'$ ) and between  $\mathbf{l}'$  and  $\mathbf{j}'$  ( $\mathbf{l}'\mathbf{j}'$ ) were also examined. The results are shown as solid angle differential cross-sections (DCSs) in figure 3 for representative collision energies ( $E_T= 0.28, 0.80$  and  $1.4$  eV), which roughly correspond to low-, intermediate- and high- $E_T$  values.

---

Figure 3. Two-vector correlations for reaction (1).

---

The  $\mathbf{k}\mathbf{k}'$  DCSs (figure 3a) show similar features at all collision energies. They are quite isotropic in the range  $\mathbf{k}\mathbf{k}'= 30^\circ$ - $150^\circ$  and they present quite pronounced forward ( $\mathbf{k}\mathbf{k}'= 0^\circ$ ) and less stressed backward ( $\mathbf{k}\mathbf{k}'= 180^\circ$ ) peaks. Thus, the  $\mathbf{k}\mathbf{k}'$  DCSs show non-negligible forward behavior. This situation somewhat resembles the one expected for a microscopic mechanism evolving through a collision complex, which favors the scattering of products in all possible directions<sup>33</sup>. In that case, the longer-lived the collision complex, the more isotropic the  $\mathbf{k}\mathbf{k}'$  distribution is expected to be. For the  $\text{O}(^1\text{D}) + \text{CH}_4$  reaction the dominant mechanism is an insertion/fast elimination one<sup>9,12-13,19</sup> and the collision complexes through which the process evolves are mainly short-lived, which explains the somewhat forward feature of the calculated  $\mathbf{k}\mathbf{k}'$  DCSs. This forward feature has also been found experimentally, as shown in figure 2b, where the experimental<sup>19</sup> and QCT  $\mathbf{k}\mathbf{k}'$  angular distributions for the  $^{18}\text{OH}$  product at  $E_T = 0.28$  eV are compared. The agreement between theory and experiment is excellent in this case. This is confirmed by the calculated velocity-scattering angle distribution for the  $^{18}\text{OH}$  product (figure 2c). The maps show the existence of backward and, especially, forward peaks. The experimental center of mass product flux 3D map depicted in figure 7 of ref. 19 for  $E_T=0.28$  eV has very similar features.

Despite the similarity between the  $\mathbf{k}\mathbf{k}'$  DCSs at different  $E_T$  values, some discrepancies arise when increasing the collision energy. For low and intermediate values of  $E_T$  ( $E_T < 1.0$  eV) the forward feature of the  $\mathbf{k}\mathbf{k}'$  angular distributions remains nearly constant as the collision energy rises. Otherwise, the scattering in the forward hemisphere is accentuated for higher values of  $E_T$ . As energy increases the system can evolve from reactants to products through more repulsive regions of the PES, which would lead to progressively more backward scattering. However, in reaction (1) the impulsive effect dominates and because of this a tendency to more forward scattering is observed as  $E_T$  increases. This trend is illustrated by the values of the average scattering angle ( $\langle\theta_{\mathbf{k}\mathbf{k}'}\rangle$ ) and the ratio of OH products scattered in the forward ( $\theta_{\mathbf{k}\mathbf{k}'} <$

90°) and backward ( $\theta_{\mathbf{k}\mathbf{k}'} > 90^\circ$ ) hemisphere (*f/b* scattering ratio). For  $E_T = 0.21, 0.80$  and  $1.4$  eV, we obtained  $\langle \theta_{\mathbf{k}\mathbf{k}'} \rangle = 75.3^\circ, 76.4^\circ, 68.9^\circ$  and *f/b* = 1.7, 1.6, 2.0, respectively.

The  $\mathbf{l}'\mathbf{j}'$  DCSs are depicted in figure 3b. They are mainly symmetric with a minimum at 90° and two maxima at 0° and 180°, which means that the  $\mathbf{l}'$  and  $\mathbf{j}'$  vectors have some tendency towards parallel alignment. For low and intermediate values of  $E_T$  the  $\mathbf{l}'\mathbf{j}'$  DCSs have a slightly antiparallel orientation ( $\theta_{\mathbf{l}'\mathbf{j}'} > 90^\circ$ ), which is softened as collision energy increases. For high- $E_T$  values the  $\mathbf{l}'\mathbf{j}'$  distributions display a preferred parallel orientation ( $\theta_{\mathbf{l}'\mathbf{j}'} < 90^\circ$ ). The values of the average  $\mathbf{l}'\mathbf{j}'$  angle ( $\langle \theta_{\mathbf{l}'\mathbf{j}'} \rangle$ ) and the ratio between parallel and antiparallel arrangement of the two vectors (*p/ap* scattering ratio) were  $\langle \theta_{\mathbf{l}'\mathbf{j}'} \rangle = 99.0^\circ, 92.5^\circ, 81.3^\circ$  and *p/ap* = 0.70, 0.89, 1.4 for  $E_T = 0.21, 0.80$  and  $1.4$  eV. As a result of the angular momenta transformation, the  $\mathbf{l}\mathbf{j}'$  correlation was similar to that described for  $\mathbf{l}'\mathbf{j}'$ .

The  $\mathbf{k}\mathbf{j}'$  and  $\mathbf{k}'\mathbf{j}'$  DCSs collected in figures 3c and 3d respectively, and correspond to symmetric distributions, as they must be. They are also quite isotropic, though slightly peaked at 90°, as expected due to the above-mentioned tendency of the system to align the  $\mathbf{j}'$  vector parallel to  $\mathbf{l}$  and  $\mathbf{l}'$ . No significant changes for the  $\mathbf{k}\mathbf{j}'$  and  $\mathbf{k}'\mathbf{j}'$  DCSs were observed as  $E_T$  increased.

The previously described slight trend of the  $\mathbf{k}$  and  $\mathbf{j}'$  vectors to be perpendicular can also be inferred from the analysis of the OH rotational alignment parameter ( $A_0^{(2)} \equiv \langle 3\cos^2\theta_{\mathbf{k}\mathbf{j}'} - 1 \rangle$ ), whose limiting values correspond to a fully perpendicular ( $A_0^{(2)} = -1$ ) or parallel ( $A_0^{(2)} = +2$ )  $\mathbf{k}\mathbf{j}'$  alignment. Here small negative values of  $A_0^{(2)}$  were found for all collision energies considered, thus suggesting a slight tendency for perpendicular  $\mathbf{k}\mathbf{j}'$  polarization. For instance,  $A_0^{(2)} = -0.092, -0.090$  and  $-0.12$  for  $E_T = 0.21, 0.80$  and  $1.4$  eV, respectively. This weak tendency for perpendicular alignment does not change with the internal state of the OH product, in contrast with the  $\text{H} + \text{H}_2\text{O} \rightarrow \text{OH} + \text{H}_2$ <sup>34</sup> and  $\text{O}(^3\text{P}) + \text{CH}_4 \rightarrow \text{OH} + \text{CH}_3$ <sup>31,35</sup> reactions (abstraction-like processes), which showed more negative values of  $A_0^{(2)}$  as higher OH rotational states were considered.

We also analysed the OH state-specific two-vector properties arising from reaction (1). We focused on the  $E_T = 0.40$  eV condition, for which some experimental results have been reported about the state-specific stereodynamics of the  $\text{O}(^1\text{D}) + \text{CH}_4$  reaction<sup>14-18</sup>: the  $\text{OH}(v'=0, N'=5)$  and  $\text{OH}(v'=4, N'=8)$   $\mathbf{k}\mathbf{k}'$  DCSs. The QCT and experimental state-specific  $\mathbf{k}\mathbf{k}'$  DCSs were previously compared using PES2<sup>24</sup>. Here we investigated other two-vector correlations for these state-specific reaction channels. We found an  $\mathbf{l} \rightarrow \mathbf{l}'$  transformation, as obtained for the full reaction. The calculated  $\mathbf{l}'\mathbf{j}'$  DCSs are essentially symmetric and exhibit pronounced peaks at 0°

and  $180^\circ$ . The  $\mathbf{k}\mathbf{j}'$  and  $\mathbf{k}'\mathbf{j}'$  distributions are also symmetric (as they must be), showing slight maxima at  $90^\circ$ . The  $A_0^{(2)}(\mathbf{k}\mathbf{j}')$  parameter takes small negative values for the two state-specific reaction channels:  $-0.11$  ( $\text{OH}(v'=0, N'=5)$ ) and  $-0.075$  ( $\text{OH}(v'=4, N'=8)$ ). A slight tendency of the system to arrange the  $\mathbf{k}'$  and  $\mathbf{j}'$  vectors perpendicularly was also been observed in the experiments for the  $\text{OH}(v'=0, N'=5)$  channel<sup>16</sup>.

#### 4. MICROSCOPIC REACTION MECHANISM

To improve our understanding on the dynamics of the title reaction the microscopic mechanism was studied. We analysed the temporal dependence of the interatomic distances and angles, and of the potential energy of the system for the reactive trajectories obtained at a range of values of  $E_T$ . The evolution from reactants to products followed two different reaction pathways: (a) insertion of the oxygen atom into a C-H bond to yield the methanol minimum followed by the dissociation of the resulting collision complex (insertion); (b) direct abstraction of a hydrogen atom by the oxygen atom (abstraction).

To separate the reactive trajectories corresponding to the two reaction pathways, the minimal value of the potential energy reached by each reactive trajectory was analysed. Abstraction trajectories evolved from reactants to products with a minimum potential energy above  $-7.0$  eV (the potential energies at the equilibrium geometries of reactants,  $\text{OH} + \text{CH}_3$  products and  $\text{CH}_3\text{OH}$  minimum are, respectively,  $-4.79$ ,  $-6.47$ , and  $-10.54$  eV). On the other hand, the insertion trajectories take minimal potential energies below  $-9.0$  eV, and most of them present values lower than  $-10.0$  eV.

At this point, it might be objected that the energy criterion chosen to discern between insertion- and abstraction-type reactive trajectories is somewhat misleading, as it implies that the abstraction trajectories penetrate the  $\text{CH}_3\text{OH}$  well to a certain extent (*ca.*  $0.5$  eV). However, the following findings should be considered to clarify this point: (a) a non-negligible influence of the deep  $\text{CH}_3\text{OH}$  minimum was found at the *ab initio* level (and then reproduced by the analytical PES), even for the “pure” abstraction pathway leading from reactants to products (i.e., for a fixed O-H- $\text{CH}_3$  collinear arrangement). This was evidenced by the presence of a shallow “minimum” (not a true minimum but a reflex of the  $\text{CH}_3\text{OH}$  minimum) located at the exit channel of the collinear abstraction pathway. Therefore, the minimal potential energy value that should be expected for the abstraction reactive trajectories is not that corresponding to the products asymptote ( $-6.47$  eV) but to the energy value of the “minimum” ( $-6.70$  eV for a O-H- $\text{CH}_3$  collinear geometry); (b) although the energy threshold chosen to select the abstraction reactive trajectories was  $-7.0$  eV, the minimal energy value calculated for nearly all of these

trajectories was higher than  $-6.75$  eV, as expected taking into account the “minimum” in the abstraction pathway.

The relative contributions to the global reactivity calculated for the two microscopic mechanisms at the  $E_T$  values considered are shown in table 2. The insertion mechanism is the main reaction pathway, although the contribution of the abstraction mechanism, which is almost negligible at  $E_T= 0.21, 0.28$  and  $0.40$  eV, increases with  $E_T$  and reaches a value of  $0.31$  at  $1.4$  eV (figure 4a). This agrees with the experimental evidence that suggests that the  $O(^1D) + CH_4$  reaction mainly evolves through insertion<sup>9,12-13,19</sup>.

---

Table 2. Microscopic mechanisms yields.

---

Figure 4. Scalar properties for the insertion and abstraction mechanisms.

---

The dynamical properties of the insertion and abstraction mechanisms have been studied. This has allowed us to obtain a deep insight on the two mechanisms and to discern whether the abstraction should be considered as a rebound or a stripping mechanism.

The dependence of the reaction probability on the impact parameter is different for the insertion and abstraction reaction mechanisms. Thus, trajectories evolving through abstraction are favored for higher values of  $b$  than insertion trajectories. The opacity functions corresponding to the insertion and abstraction mechanisms for  $E_T= 1.0$  eV are plotted in figure 4b. Moreover, the opacity functions associated with the insertion mechanism shift to higher values of  $b$  as  $E_T$  rises. This finding, along with the increasing contribution of the abstraction mechanism with  $E_T$ , explains that the global reactivity for reaction (1) appears for larger values of  $b$  as collision energy rises (figure 1b).

The OH vibrational distributions corresponding to the insertion and abstraction mechanisms at  $E_T= 0.6$  and  $1.4$  eV are shown in figures 4c-d. The results depend on the reaction pathway: abstraction trajectories yield highly inverted vibrational distributions, while insertion trajectories give much less OH vibrational excitation. This is expected for the two types of microscopic mechanisms in the case of an exothermic reaction<sup>33</sup>. Both the insertion and abstraction OH vibrational distributions become quite more excited as  $E_T$  rises, due to the increase in available energy. For abstraction, the OH vibrational population maximum appears at  $v'=4$  for  $E_T= 0.40$  and  $0.60$  eV, and at  $v'=5$  for  $E_T= 0.80, 1.0$  and  $1.4$  eV. Similarly, the insertion OH vibrational distributions peak at  $v'=0$  for  $E_T= 0.21, 0.40, 0.60$  and  $0.80$  eV, at  $v'=1$  for  $E_T=$

1.0 eV, and at  $v'=2$  for  $E_T= 1.4$  eV. This finding and the increasing contribution of abstraction as  $E_T$  increases explain the dependence of the global OH vibrational distribution on the collision energy (figure 1d and table 1).

There are also differences between the insertion and abstraction mechanisms in the case of the OH rotation. The insertion trajectories display excited OH rotational distributions peaking at high- $N'$  values for all populated vibrational levels. Moreover, they become more excited as  $E_T$  increases. On the other hand, the shape of the rotational distributions arising from the abstraction mechanism depends on the vibrational level. For the lowest vibrational levels ( $v' \leq 4$ ) excited distributions similar to the insertion ones were obtained, while less excited rotational distributions peaking at low- $N'$  values appeared for the highest vibrational levels ( $v' \geq 5$ ). These trends are shown in figures 4e-f, where the insertion and abstraction OH( $v'=3, 5$ ) rotational distributions are depicted for  $E_T = 1.4$  eV. For  $v'=3$  as the insertion and abstraction trajectories lead to similar OH rotational distributions, a unimodal and quite excited global rotational distribution is found. The different behavior of the insertion and abstraction reaction modes for  $v'=5$ , however, results in a clearly bimodal OH full rotational distribution, which peaks at low- $N'$  values since the abstraction mechanism is the most important one producing OH( $v' \geq 5$ ) for  $E_T= 1.4$  eV. For these excited OH vibrational levels, the abstraction mechanism yields low excited rotational distributions in all cases, while insertion leads to more excited rotational distributions as  $E_T$  rises. This finding and the increasing contribution of the abstraction mode as the collision energy increases, explains why the bimodal feature of the OH( $v' \geq 5$ ) rotational distributions becomes stressed as  $E_T$  rises (figure 1f).

The two-vector correlations corresponding to the insertion and abstraction pathways have also been analysed separately. Figure 5 shows the  $\mathbf{k}\mathbf{k}'$  DCSs corresponding to the two different mechanisms at  $E_T= 0.60$  and 1.40 eV. Clearly, abstraction leads to pronounced forward distributions, while insertion furnishes more symmetric scattering, though with a forward predominance too. This together with the finding that the abstraction mechanism was favored for high- $b$  values, allowed us to classify this reaction mode as stripping-type. On the other hand, the insertion mechanism furnishes more symmetric scattering, though with a forward predominance too. The deviation of the insertion  $\mathbf{k}\mathbf{k}'$  DCSs from the isotropic situation expected for this mechanism is explained by the short lifetimes of the collision complexes. The forward feature of the insertion  $\mathbf{k}\mathbf{k}'$  DCSs decreases slightly as  $E_T$  increases, though its effect on the global  $\mathbf{k}\mathbf{k}'$  DCSs is counterbalanced by the increasing contribution of abstraction. This explains why the forward behavior of the global  $\mathbf{k}\mathbf{k}'$  DCSs become stressed for higher collision energies (figure 3a).

---

Figure 5.  $\mathbf{k}\mathbf{k}'$  DCSs for the insertion and abstraction mechanisms.

---

Similarly, in the case of the  $\mathbf{l}'\mathbf{j}'$  correlation the parallel feature of the DCSs corresponding to the abstraction mechanism explains the increasing parallel behavior of the full  $\mathbf{l}'\mathbf{j}'$  DCS with  $E_T$  (figure 3b). For the  $\mathbf{k}\mathbf{j}'$  and  $\mathbf{k}'\mathbf{j}'$  correlations, minor differences were found between the two mechanisms. Thus, similar values of the rotational alignment parameter were found for the insertion- and abstraction-like trajectories, which did not show variations of the  $A_0^{(2)}$  value with the final state of the OH product. As mentioned in section 3.2, this situation differs from the behavior established for the  $\text{H} + \text{H}_2\text{O} \rightarrow \text{OH} + \text{H}_2$ <sup>34</sup> and  $\text{O}(^3\text{P}) + \text{CH}_4 \rightarrow \text{OH} + \text{CH}_3$ <sup>31,35</sup> reactions. However, it must be taken into account that these two processes evolve through abstraction mechanisms which are mainly of rebound-type (i.e., they are favored for low- $b$  values and yield backward  $\mathbf{k}\mathbf{k}'$  angular distributions), while the  $\text{O}(^1\text{D}) + \text{CH}_4$  reaction proceeds *via* insertion and stripping-type abstraction (i.e., it is favored for high- $b$  values and yields forward  $\mathbf{k}\mathbf{k}'$  angular distributions) mechanisms. In the  $\text{O}(^3\text{P}) + \text{CH}_4 \rightarrow \text{OH} + \text{CH}_3$ <sup>35</sup> reaction those reactive trajectories with non-rebound feature do not display such a strong dependence of  $A_0^{(2)}$  with the final internal state of the OH product. This tendency may correlate with the stronger  $\mathbf{l}'\mathbf{j}'$  parallel alignment found for the rebound mechanism than for the non-rebound one, although this is not completely clear.

## 5. SUMMARY AND CONCLUDING REMARKS

A study of the collision energy effects on the dynamics of the  $\text{O}(^1\text{D}) + \text{CH}_4 \rightarrow \text{OH} + \text{CH}_3$  reaction has been performed using the quasiclassical trajectory method on an analytical triatomic potential energy surface previously derived in our group for this system. The scalar and two-vector properties of the reaction have been analyzed in terms of the collision energy, considering the following  $E_T$  values: 0.21, 0.28, 0.40, 0.60, 0.80, 1.0 and 1.4 eV. At  $E_T=0.28$  eV the QCT results showed a good agreement with very recent experimental data on the products translational energy distribution,  $^{18}\text{OH}$   $\mathbf{k}\mathbf{k}'$  differential cross-section (DCS) and  $^{18}\text{OH}$  velocity-scattering angle distribution. Two different microscopic reaction mechanisms have been found to contribute to the reactivity: an insertion mechanism and an abstraction mechanism, the former being the most important one though the latter increases its contribution as  $E_T$  rises. The features of the dependence of the global dynamical behavior of the system on the collision energy can be explained in terms of the different dynamical properties observed for each mechanism.

## **Acknowledgments**

This study was supported by the "Dirección General de Enseñanza Superior" of the Spanish Ministry of Education and Culture through the DGES projects refs. PB98-1209-C02-01 and -02. Financial support from the "Generalitat de Catalunya" (Autonomous Government of Catalonia) ref. 2000SGR 00016 is also acknowledged. J.H. thanks to the CIRIT from the "Generalitat de Catalunya" for a predoctoral research grant. The authors are also grateful to the "Centre de Supercomputació i Comunicacions de Catalunya (C4-CESCA/CEPBA)" for computer time.

Table 1. Vibrational populations and average rotational levels of the OH product arising from the  $O(^1D) + CH_4 \rightarrow OH + CH_3$  reaction <sup>a),b),c)</sup>.

$E_T / \text{eV}$	$P(v') \ \& \ \langle N' \rangle_{v'}$							
	$v'=0$	$v'=1$	$v'=2$	$v'=3$	$v'=4$	$v'=5$	$v'=6$	$v'=7$
0.21	0.26 (18.3)	0.25 (16.6)	0.23 (13.8)	0.18 (11.1)	0.08 (7.2)			
0.28	0.27 (18.8)	0.25 (17.2)	0.21 (14.2)	0.18 (11.5)	0.09 (7.9)	0.003 (3.0)		
0.40	0.27 (19.9)	0.24 (18.2)	0.20 (15.5)	0.18 (12.7)	0.10 (9.3)	0.01 (5.3)		
0.60	0.24 (21.5)	0.22 (19.6)	0.20 (17.0)	0.17 (14.3)	0.12 (10.3)	0.05 (6.7)	$5 \times 10^{-4}$	
0.80	0.19 (22.5)	0.19 (20.6)	0.18 (18.2)	0.17 (15.8)	0.16 (12.6)	0.10 (7.8)	0.01 (5.0)	
1.0	0.15 (23.8)	0.16 (21.4)	0.16 (19.5)	0.16 (17.1)	0.17 (13.7)	0.16 (8.4)	0.03 (6.2)	$2 \times 10^{-4}$
1.4	0.11 (26.0)	0.12 (23.7)	0.13 (21.5)	0.15 (19.5)	0.18 (15.8)	0.21 (10.1)	0.09 (8.0)	0.01 (7.4)

<sup>a)</sup> For each condition and vibrational level, the first value given corresponds to the vibrational population, while the second one in parentheses is the average rotational level.

<sup>b)</sup> For some of the highest OH populated vibrational levels there was not enough statistics to obtain reliable values of the average rotational levels.

<sup>c)</sup> The average statistical errors (one standard deviation) corresponding to the vibrational populations and the average rotational levels are less than 1 and 5%, respectively.

Table 2. Microscopic mechanisms yields for the  $O(^1D) + CH_4 \rightarrow OH + CH_3$  reaction <sup>a)</sup>.

$E_T / eV$	Mechanism	
	Abstraction	Insertion
0.21	0	1
0.28	$9 \times 10^{-4}$	1
0.40	0.01	0.99
0.60	0.04	0.96
0.80	0.11	0.89
1.00	0.21	0.79
1.40	0.31	0.69

<sup>a)</sup> Normalized to unity.

## FIGURE CAPTIONS

**Figure 1.** (a) Excitation function for the global  $O(^1D) + CH_4$  reaction ( $\dot{E}$ ) and for the OH channel (reaction (1);  $\mathcal{C}$ ); (b) Opacity function for reaction (1) at  $E_T = 0.28$  ( $\tilde{N}$ ),  $0.80$  ( $\mathring{A}$ ), and  $1.4$  ( $\ddot{U}$ ) eV; (c) average fractions of the available energy for reaction (1) channeled as products vibration ( $\hat{a}$ ), rotation ( $\ddot{O}$ ) and translation ( $\hat{a}$ ); (d) OH vibrational distributions for  $E_T = 0.28$  ( $\tilde{N}$ ),  $0.80$  ( $\mathring{A}$ ) and  $1.4$  ( $\ddot{U}$ ) eV; (e-f) OH( $v'=0, 5$ ) rotational distributions for  $E_T = 0.28$  ( $\tilde{N}$ ),  $0.80$  ( $\mathring{A}$ ) and  $1.4$  ( $\ddot{U}$ ) eV. The opacity functions, vibrational and rotational distributions are normalized to unit area. The statistical errors (one standard deviation) are less than 5% in case of the rotational distributions and less than 1% for the other properties.

**Figure 2.** (a-b) Experimental (—, ref. 19) and QCT ( $\tilde{N}$ ) products relative translational energy distributions (a) and  $\mathbf{k}\mathbf{k}'$  angular distributions expressed as solid angle differential cross-sections (b) of reaction (1) at  $E_T = 0.28$  eV. All distributions are normalized to unit area. The statistical errors of the QCT results (one standard deviation) are less than 1%. (c) Velocity-scattering angle distributions for the  $^{18}OH$  product expressed as a 3D map as well as a contour map.

**Figure 3.** (a)  $\mathbf{k}\mathbf{k}'$ , (b)  $\mathbf{l}'\mathbf{j}'$ , (c)  $\mathbf{k}\mathbf{j}'$  and (d)  $\mathbf{k}'\mathbf{j}'$  two-vector angular distributions of reaction (1) expressed as solid angle differential cross-sections for  $E_T = 0.28$  eV ( $\tilde{N}$ ),  $0.80$  eV ( $\mathring{A}$ ) and  $1.4$  eV ( $\ddot{U}$ ). All distributions are normalized to unit area. The statistical errors (one standard deviation) are less than 1%.

**Figure 4.** Global (—), insertion ( $\mathcal{C}$ ) and abstraction ( $\dot{E}$ ) scalar properties of reaction (1): (a) excitation functions; (b) opacity functions for  $E_T = 1.0$  eV; (c-d) OH vibrational distributions for  $E_T = 0.60$  and  $1.4$  eV, respectively; (e-d) OH( $v'=3, 5$ ) rotational distributions for  $E_T = 1.4$  eV, respectively. Global opacity functions, and vibrational and rotational distributions are normalized to unit area. The statistical errors (one standard deviation) are less than 5% in case of the rotational distributions and less than 1% for the other properties.

**Figure 5.** Global (—), insertion ( $\mathcal{C}$ ) and abstraction ( $\dot{E}$ )  $\mathbf{k}\mathbf{k}'$  solid angle differential cross-sections of reaction (1) for  $E_T = 0.60$  and  $1.4$  eV. Global distributions are normalized to unit area. The statistical errors (one standard deviation) are less than 1%.

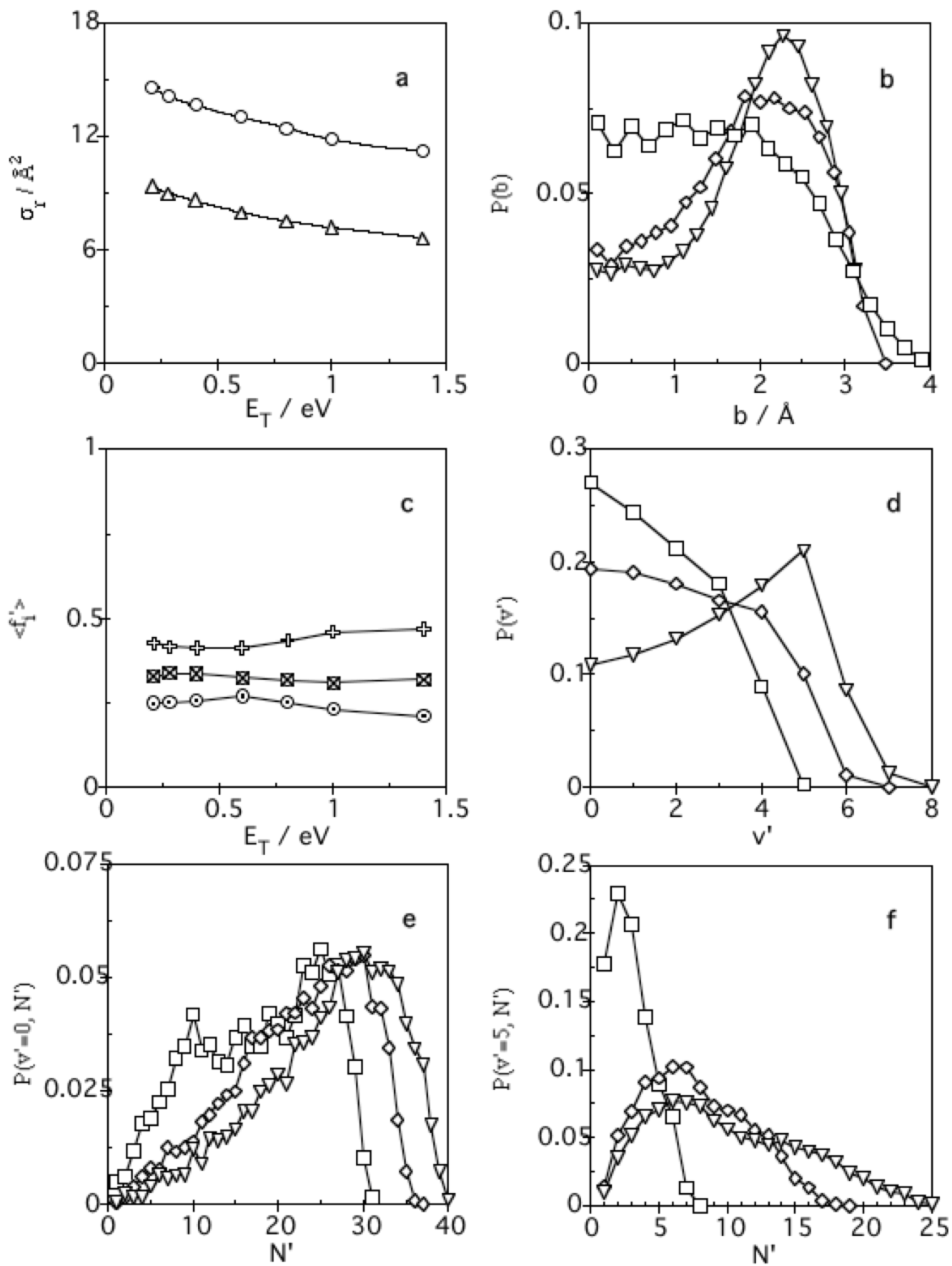
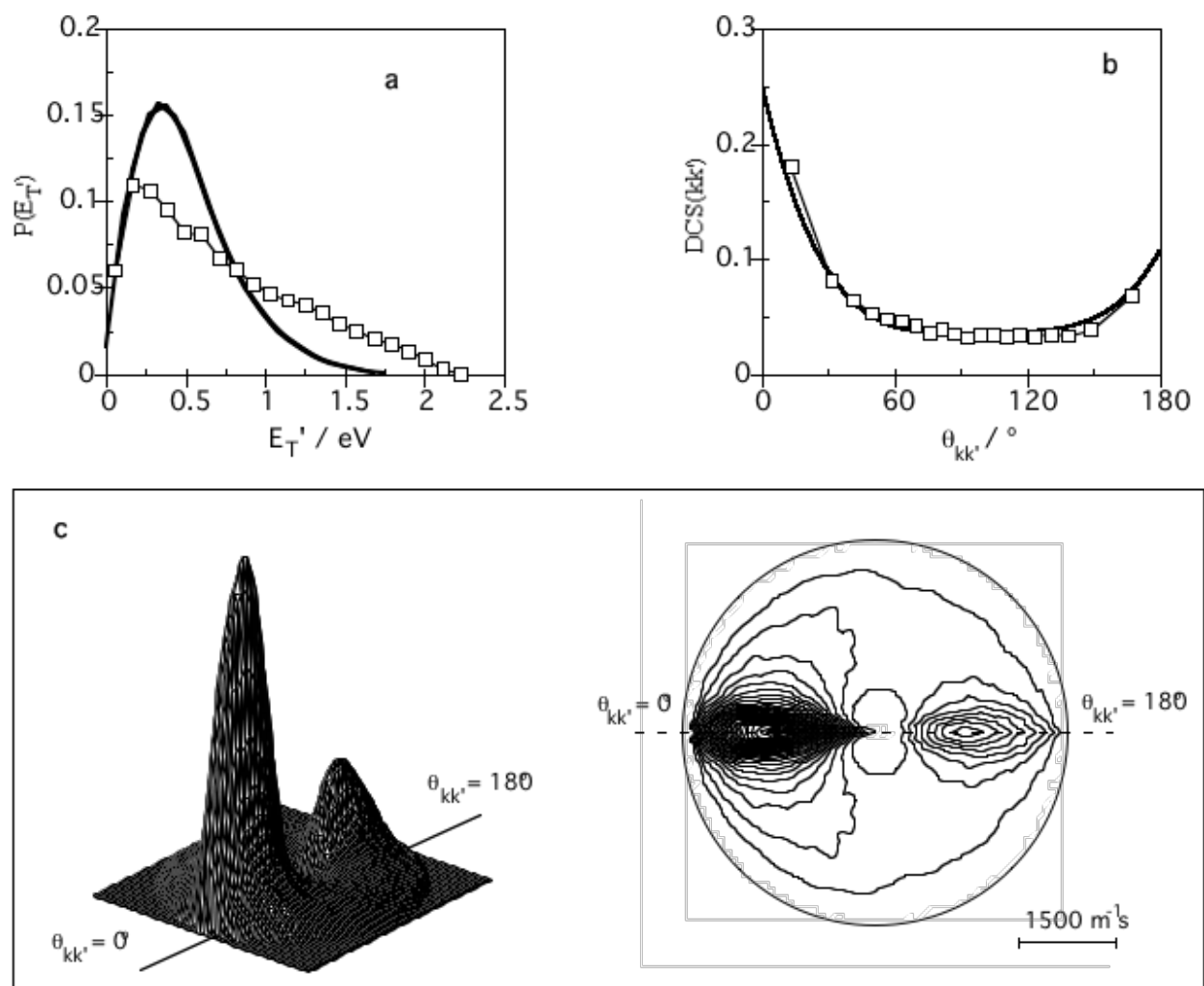


FIGURE 1



**FIGURE 2**

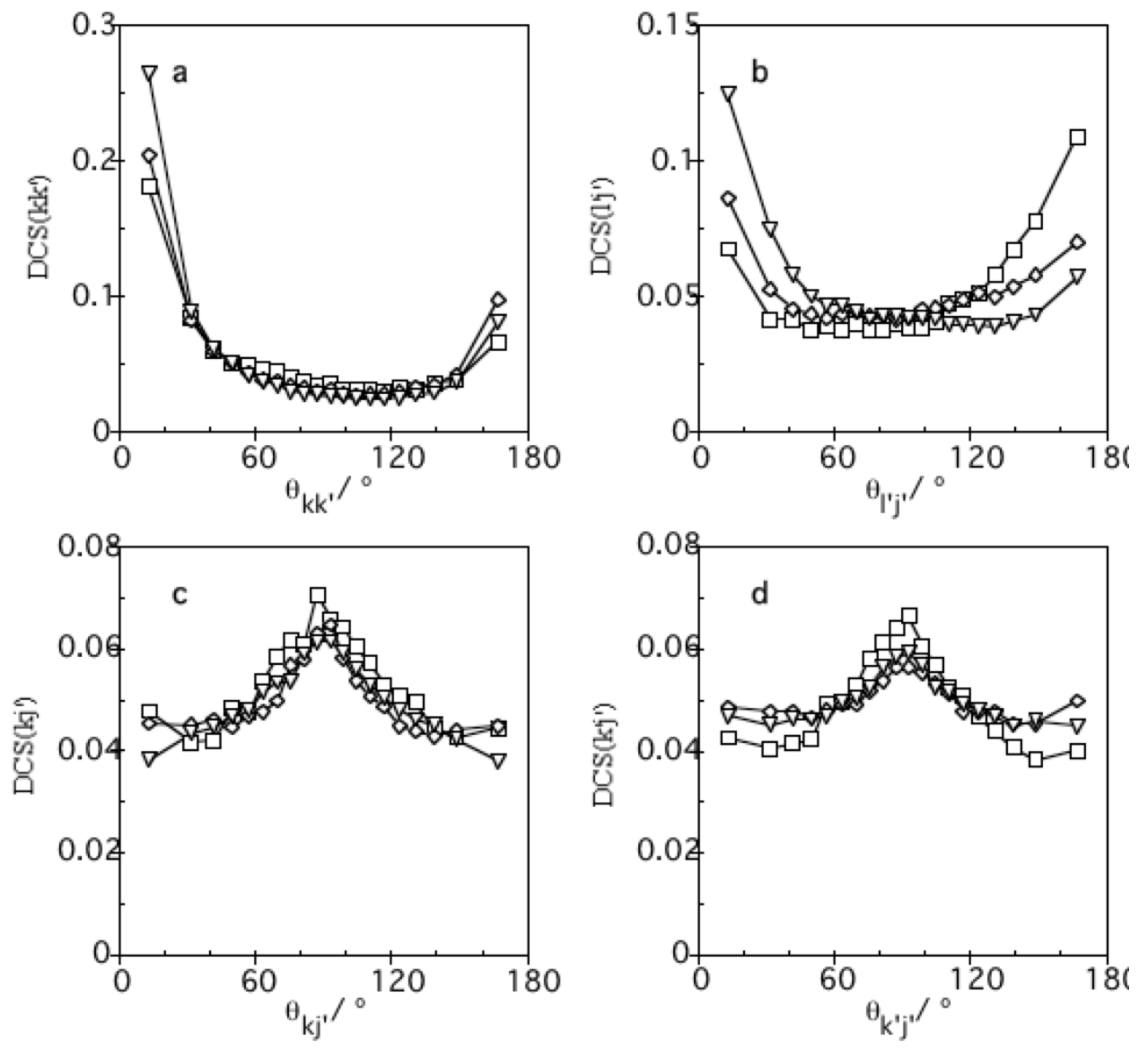


FIGURE 3

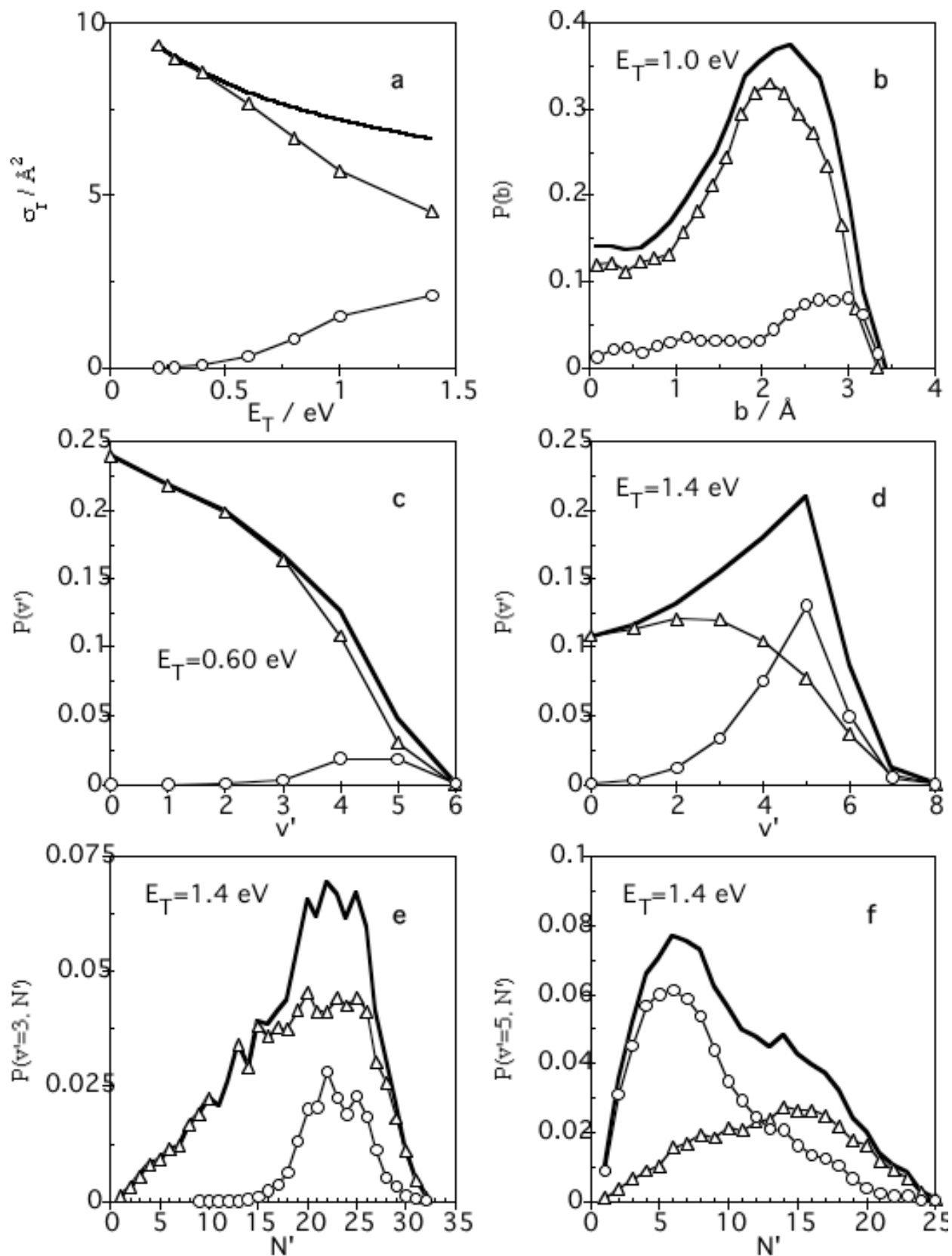


FIGURE 4

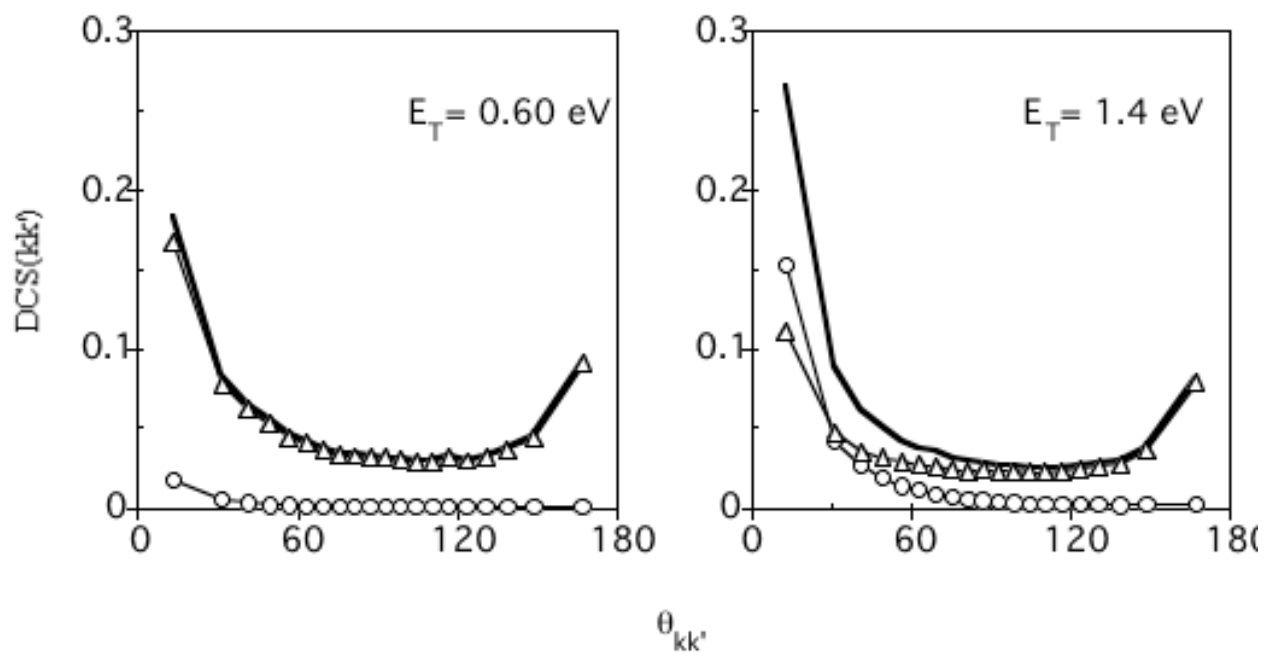


FIGURE 5

## References

- <sup>1</sup> M.W. Chase, Jr., C.A. Davies, J.R. Downey, Jr., D.J. Frurip, R.A. McDonald, and A.N. Syverud, *J. Phys. Chem. Ref. Data* **14** Suppl. 1 (1985).
- <sup>2</sup> J.R. Wiesenfeld, *Acc. Chem. Res.* **15** (1982) 110.
- <sup>3</sup> P. Warneck, *Chemistry of the Natural Atmosphere*, Academic, San Diego, 1988.
- <sup>4</sup> E.B. Burnett and C.R. Burnett, *J. Atmos. Chem.* **21** (1995) 13.
- <sup>5</sup> R. Atkinson, D.L. Baulch, R.A. Cox, R.F. Hampson Jr., J.A. Kerr, M.J. Rossi, and J. Troe, *J. Phys. Chem. Ref. Data* **28** (1999) 206 and references therein.
- <sup>6</sup> A.C. Luntz, *J. Chem. Phys.* **73** (1980) 1143.
- <sup>7</sup> P.M. Aker, J.J.A. O'Brien, and J.J. Sloan, *J. Chem. Phys.* **84** (1986) 745.
- <sup>8</sup> S.G. Cheskis, A.A. Iogansen, P.V. Kulakov, I. Yu. Razuvaev, O.M. Sarkisov, and A.A. Titov, *Chem. Phys. Lett.* **155** (1989) 37.
- <sup>9</sup> C.R. Park and J.R. Wiesenfeld, *J. Chem. Phys.* **95** (1991) 8166.
- <sup>10</sup> Y. Rudich, Y. Hurwitz, G.J. Frost, V. Vaida, and R. Naaman, *J. Chem. Phys.* **99** (1993) 4500.
- <sup>11</sup> M. González, J. Hernando, R. Sayós, M.P. Puyuelo, P.A. Enríquez, J. Guallar, and I. Baños, *Faraday Discuss.* **108** (1997) 453.
- <sup>12</sup> S. Wada and K. Obi, *J. Phys. Chem. A* **102** (1998) 3481.
- <sup>13</sup> M. González, M.P. Puyuelo, J. Hernando, R. Sayós, P.A. Enríquez, J. Guallar, and I. Baños, *J. Phys. Chem. A* **104** (2000) 521.
- <sup>14</sup> M. Brouard, S.P. Duxon, and J.P. Simons, *Isr. J. Chem.* **34** (1994) 67.
- <sup>15</sup> M. Brouard and J.P. Simons in *The Chemical Dynamics and Kinetics of Small Radicals*, Part II, edited by K. Liu and A. Wagner, World Scientific, Singapore, 1995, p. 795.
- <sup>16</sup> M. Brouard, H.M. Lambert, J. Short, and J.P. Simons, *J. Phys. Chem.* **99** (1995) 13571.
- <sup>17</sup> M. Brouard, H.M. Lambert, C.L. Russell, J. Short, and J.P. Simons, *Faraday Discuss.* **102** (1995) 179.
- <sup>18</sup> J.P. Simons, *J. Chem. Soc. Faraday Trans.* **93** (1997) 4095.
- <sup>19</sup> J.J. Lin, J. Shu, Y.T. Lee, and X. Yang, *J. Chem. Phys.* **113** (2000) 5287.
- <sup>20</sup> T. Suzuki and E. Hirota, *J. Chem. Phys.* **98** (1993) 2387.
- <sup>21</sup> R. Schott, J. Schlütter, M. Olzmann, and K. Kleinermanns, *J. Chem. Phys.* **102** (1995) 8371.
- <sup>22</sup> H. Arai, S. Kato, and S. Koda, *J. Phys. Chem.* **98** (1994) 12.
- <sup>23</sup> M. González, J. Hernando, I. Baños, and R. Sayós, *J. Chem. Phys.* **111** (1999) 8913.
- <sup>24</sup> M. González, J. Hernando, M.P. Puyuelo, and R. Sayós, *J. Chem. Phys.* **113** (2000) 6748.

- <sup>25</sup> R.N. Porter and L.M. Raff in *Dynamics of Molecular Collisions, Part B*, edited by W.H. Miller, Plenum, New York, 1976, p. 1.
- <sup>26</sup> D.G. Truhlar and J.T. Muckerman in *Atom-molecule Collision Theory: A Guide For The Experimentalist*, edited by R.B. Bernstein, Plenum, New York, 1979, p. 505.
- <sup>27</sup> H.R. Mayne, *Int. Rev. Phys. Chem.* **10** (1991) 107.
- <sup>28</sup> R. Sayós and M. González, TRIQCT (unpublished program).
- <sup>29</sup> M. González, D. Troya, M.P. Puyuelo, R. Sayós, and P.A. Enríquez, *Chem. Phys. Lett.* **300** (1999) 603.
- <sup>30</sup> M. González, J. Hernando, J. Millán, and R. Sayós, *J. Chem. Phys.* **110** (1999) 7326.
- <sup>31</sup> R. Sayós, J. Hernando, M.P. Puyuelo, P.A. Enríquez, and M. González, *Chem. Phys. Lett.*, **341** (2001) 608.
- <sup>32</sup> R. Sayós, C. Oliva, and M. González, *J. Chem. Phys.* **113** (2000) 6736.
- <sup>33</sup> R.D. Levine and R.B. Bernstein, *Molecular Reaction Dynamics*, Oxford University Press, New York, 1987.
- <sup>34</sup> D. Troya, G. Lendvay, M. González, and G.C. Schatz, *Chem. Phys. Lett.*, **343** (2001) 420.
- <sup>35</sup> M. González, J. Hernando, and R. Sayós, unpublished.